ARMOR DAMAGE ON HARBOR SIDE RUBBLE MOUND OF COMPOSITE BREAKWATERS AGAINST WATER JET CAUSED BY IMPINGING BORE-LIKE TSUNAMI

Sohei Maruyama[1] , Jun Mitsui[1] , Akira Matsumoto[1] and Minoru Hanzawa[1]

A series of hydraulic model experiments was systematically and carefully carried out to estimate the stability of various types of armor units for a harbor-side rubble mound of a composite breakwater against a water jet caused by an impinging bore-like tsunami. Armor stones of weight 1 ton were seen to be easily removed by the tsunami flow. Flat type concrete blocks with well-arranged holes showed high stability. In the case of using wave-dissipating blocks, the total stability of the armor layer was enhanced by placing heavier blocks along the toe of the slope. Numerical analysis was also carried out to investigate the effect of the shape of the blocks. The computed time series of water level and the behavior of the impinging jet agreed well with the experimental ones. The computational result of hydrodynamic forces acting on armor blocks revealed that the uplift forces were largely decreased by the holes in the blocks.

Keywords: Tsunami; water jet; rubble-mound of composite breakwaters; armor unit

INTRODUCTION

Many breakwaters were damaged by the tsunami generated by the Great East Japan Earthquake on March 11th, 2011. One of the causes of damage was scouring of the harbor-side rubble mound due to overflow from the tsunami as shown in Figure 1. This was a formerly inconceivable type of failure (Ministry of Land, Infrastructure, Transport and Tourism 2013). Studies on the detailed mechanism of the failure are now being conducted. For example, Arikawa et al. (2013) conducted a hydraulic model experiment to reproduce the failure of the breakwaters. They confirmed that the failure of the breakwater at the port of Hachinohe was collapse due to scouring.

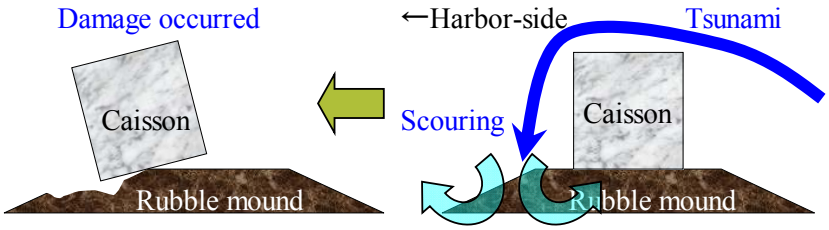

Figure 1. Damage of a breakwater due to scouring

As a countermeasure against large tsunami in the future, reinforcement of the harbor-side mound using additional rubble stones is showing promise. Figure 2 shows one of the proposed measures against tsunami. The additional rubble stones will not only delay the progress of scouring but also enhance the resistance against tsunami force. Large stones or concrete blocks with sufficient stability will be required to cover the surface of the reinforced mound because the reinforced mound will be exposed to the severe action of a water jet caused by the impinging bore-like tsunami.

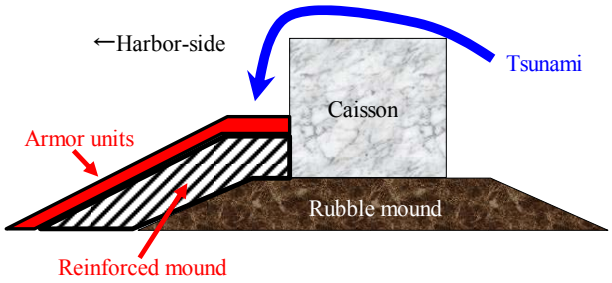

Figure 2. One of the proposed measures to water jet caused by impinging bore-like tsunami

[1] Technical Research Institute , Fudo Tetra Corporation, 2-7, Higashi-nakanuki, Tsuchiura, Ibaraki, 300-0006, Japan

However, the stability of armor units against water jet is not understood yet. In our study, a series of hydraulic model experiments was conducted to better understand the relationship between the initial impact by the flow and stability of armor material. Numerical analysis was also conducted to investigate the effect of the shape of the blocks.

HYDRAULIC MODEL EXPERIMENTS

Experimental setup

Experiments were carried out using a 40 m long, 1 m wide and 1.2 m deep wave flume. Figure 3 shows the schematic layout of the wave flume. The breakwater model was placed on the 1/30 bottom slope.

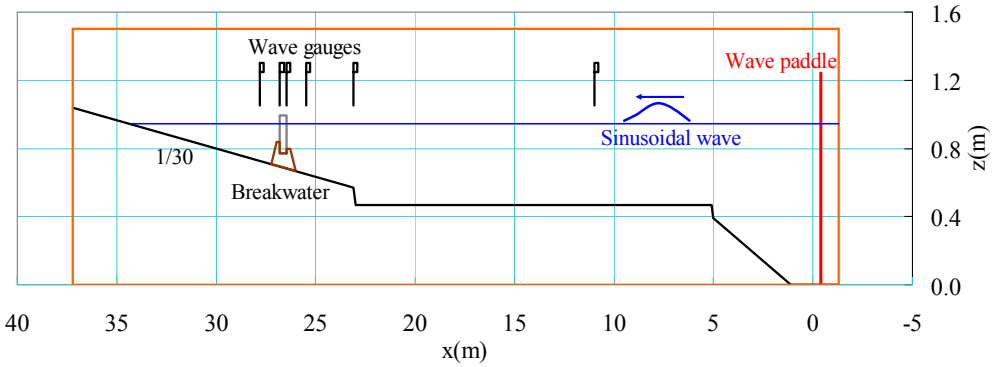

Figure 3. Wave flume overview

Figure 4 shows the cross section of the model breakwater. The model scale was set to 1/50. In the following, a prototype scale is used. In this study, the height of the reinforced mound H_M is set to about $C/3$ which includes the thickness of armor units. The crown width of the reinforced mound B_M is also adjusted depending on the type and size of the armor units. The caisson model was made of wood and was fixed with a weight so that it would not be moved by tsunami action since this study was focused on the stability of armor units.

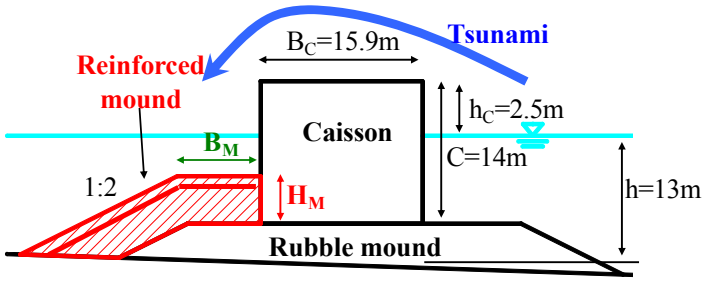

Figure 4. Cross section of the model breakwater

Table 1 shows the armor units used in the experiments. Armor stones of weight 1 ton, two kinds of flat type concrete blocks (X-Block and Permex) and wave-dissipating blocks (Tetrapod) with various weights were used. Permex was recently developed by refining X-Block. The large holes in Permex were found to contribute to high stability against wave action due to the reduction of the uplift force (Hamaguchi et al. 2007, Kubota et al. 2008).

Table 1. Armor units used in the experiments

Armor units	Mass	Shape	B_M(m)	H_M(m)
Armor stone	1.0t		6.40	4.65
Flat type concrete block-A (X-Block)	30.5t		7.90	4.65
	16.2t		6.40	
Flat type concrete block-B (Permex)	16.1t		7.40	4.65
	8.1t		5.88	
	4.1t		7.02	
Wave-dissipating concrete block (Tetrapod)	28.8t		8.30	4.80
	14.5t			

Since this study is concentrated on the understanding of the relationship between the initial impact by the flow and the stability of the armor material, tsunami was generated by a piston type wave-maker to reproduce a single hump of water. Four tsunami waves with different heights were prepared by varying the stroke of the wave paddle which followed a sinusoidal motion. Their heights of overflow were 2.1 m, 4.5 m, 5.5 m and 7.1 m. Figure 5 shows a time-series of water surface elevations measured at the position of the front face of the caisson with a breakwater in place. In this figure, h_c denotes the crown height of the breakwater above the still water level. In the stability tests, the armor units and rubble mound were not rebuilt after tsunami attack of each height. The extent of the damage to the 1.0 t armor stones was measured by using a mechanical type topography profiler. Cross sections were measured before and after each tsunami attack. In the cases of the concrete blocks, the number of the moved blocks was counted as an accumulated number.

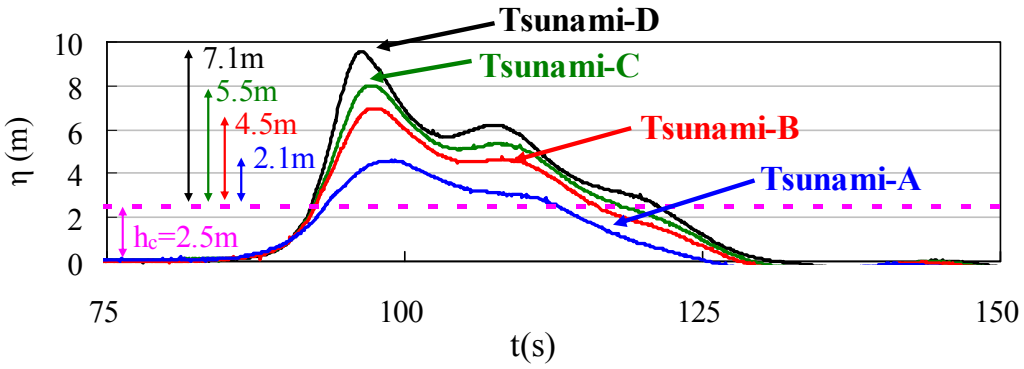

Figure 5. Time series of water surface elevation (front face of the caisson)

Overflow process of water jet

Figure 6 shows the overflow process of water jet caused by impinging bore-like tsunami, and this is the Tsunami-D shown in Figure 5. The water jet inflows from near the shoulder of the slope, and then it flows into the seabed along the slope. Finally water jet strongly impacts on both the shoulder and toe of the slope. Throughout, the strong flow migrates gradually from the shoulder to the toe of the slope.

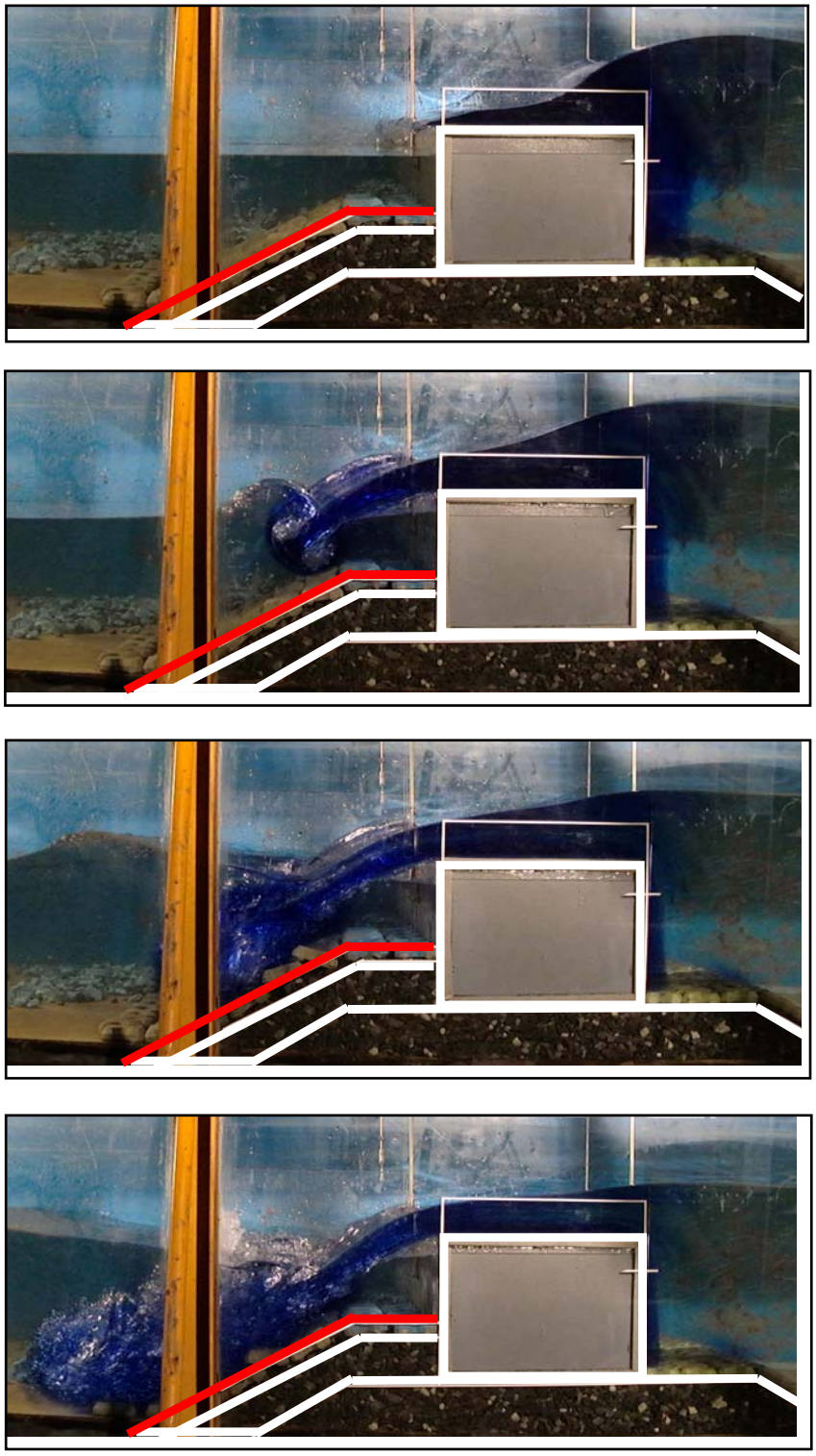

Figure 6. Overflow process of water jet caused by impinging bore-like tsunami (7.1 m overflow: tsunami-D)

Stability of 1.0 t armor stones

Figure 7 shows the cross sectional change in the reinforced mound covered with 1.0t armor stones. The damage began after the 4.5 m overflow. The whole rubble mound suffered deformation after the 7.1m overflow. Figure 8 shows the state of damage to the 1.0t armor stones. The armor stones were largely scattered and the rubble stones under the armor stones were also scoured out in this case. Thus, the 1.0 t armor stones covering the surface of the reinforced mound did not secure the stability of the reinforced mound against such heights of tsunami.

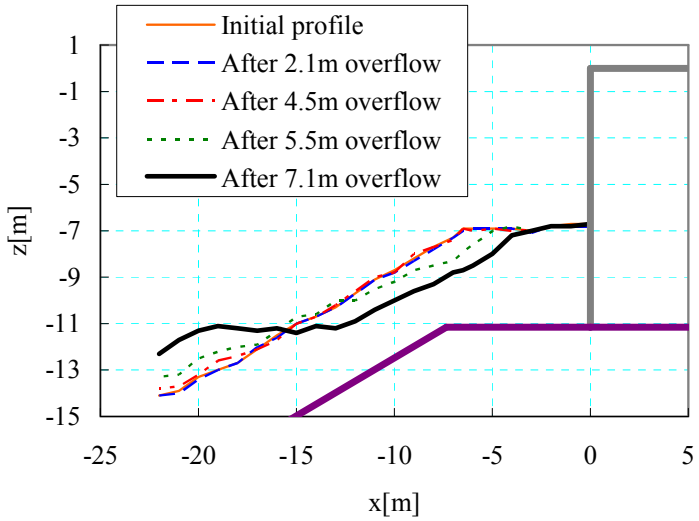

Figure 7. Cross sectional change in the reinforced mound covered with the 1.0 t armor stone

Figure 8. Damage to the 1.0 t armor stones (left: before overflow, right: after 7.1 m overflow)

Stability of X-Block

X-Block of 30.5 t and 16.2 t were used. Both sizes of blocks proved stable against 2.1 m, 4.5 m, and 5.5 m overflow. After 7.1 m overflow, serious damage was seen to concentrate at the shoulder of the slope as shown in Figure 9. As previously mentioned, the strong flow migrated gradually from the shoulder of the slope to the toe. When the strong flow hit the blocks, they were overturned.

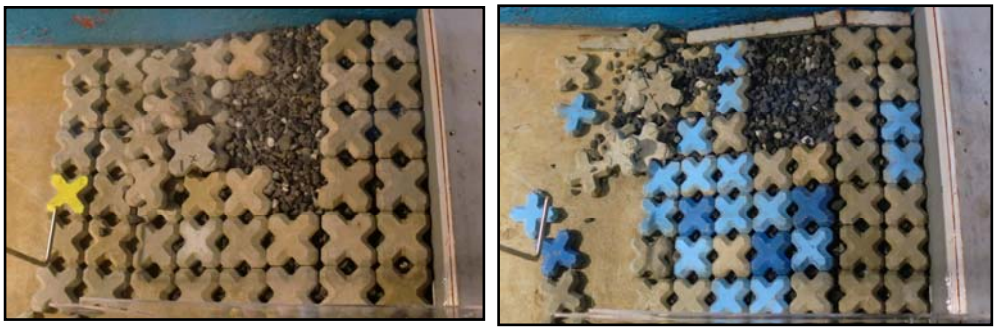

Figure 9. Damage to X-Block after 7.1 m overflow (left: 30.5 t, right: 16.2 t)

Stability of Permex

Permex of 16.1 t, 8.1 t and 4.1 t were used. This block has been developed intended to be used to cover mounds of composite breakwaters and the submerged breakwaters. It has five well-arranged holes to effectively reduce uplift forces acting on block.

The 16.1 t blocks proved stable against the highest tsunami overflow (=7.1 m) in this experiment as shown in Figure 10.

Figure 10. Result of Permex (16.1 t) after 7.1 m overflow

The 8.1 t and 4.1 t blocks were stable against 2.1 m, 4.5 m, and 5.5 m overflow. After the 7.1 m overflow, although there was damage at the toe of the slope in the form of sliding, the main part of the reinforced mound stayed stable. Figure 11 shows the state of damage to Permex of 8.1 t and 4.1 t after 7.1 m overflow. It was seen that blocks with holes reduced the uplift force and had high stability against water jet.

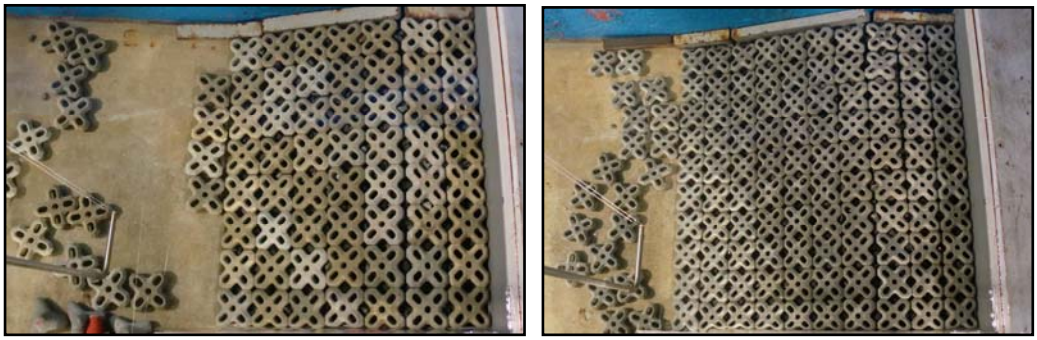

Figure 11. Damage to Permex after 7.1 m overflow (left: 8.1 t, right: 4.1 t)

Stability of Tetrapod

Tetrapod of 28.8 t and 14.5 t were used. The 28.8 t block was stable against the highest overflow (=7.1 m). Figure 12 shows the result of the 28.8 t block after 7.1 m overflow.

Figure 12. Result of Tetrapod (28.8 t) after 7.1 m overflow

The 14.5 t Tetrapod proved stable against 2.1 m, 4.5 m, and 5.5 m overflow. After 7.1 m, although there was damage to the toe of the slope in the form of sliding, the main part of the reinforced mound stayed stable. Figure 13 shows the state of damage to the 14.5 t Tetrapod after 7.1 m overflow.

For this case, a reinforced mound can be stabilized by placing heavier blocks along the toe of the slope. In this experiment, X-Block of 30.5 t was used. Figure 14 shows improved stability achieved by using this method.

Figure 13. Damage to Tetrapod (14.5 t) after 7.1 m overflow

Figure 14. Result of Tetrapod (14.5 t) reinforced by placing X-Block (30.5 t) after 7.1 m overflow

Summary on the stability of the armor units

A stability number N_{S1} for the armor units against tsunami overflow is expressed using the Hudson type formula given by:

$$N_{S1} = \frac{\eta_{\max} - h_c}{(S_r - 1)D_n} \tag{1}$$

where η_{max} is the upper limit of the height of overflow during stable, h_c is the crown height of the caisson, S_r is the specific gravity of the armor units, and D_n is the nominal diameter of the armor units ($=v^{1/3}$, v: volume of the armor units). In the following analysis, the damage at the toe of the slope was not taken into account because the armor units placed at the toe of the slope do not cover the main part of the reinforced mound.

Figure 15 shows the N_{S1} of the armor units used in this experiment. The arrow shown in Figure 15 means that Permex and Tetrapod have a larger N_{S1} because Permex and Tetrapod were not damaged by the highest tsunami overflow in this experiment. From Figure 15, it can be seen that Permex has high stability against water jet caused by impinging bore-like tsunami.

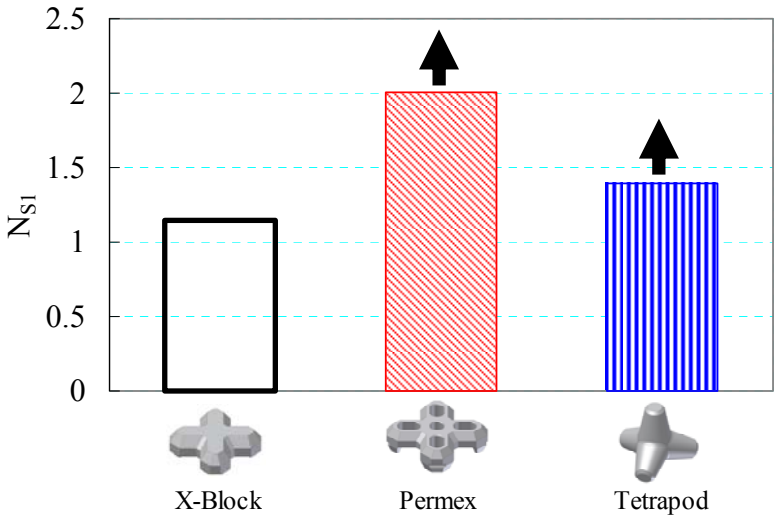

Figure 15. No-damage Stability number N_{S1} of the armor units used in this experiment

NUMERICAL ANALYSIS

Method

Permex showed high stability against water jet in the hydraulic experiment. To confirm the effect of the well-arranged five holes for reducing the uplift force acting on the block, numerical analysis was conducted.

A multiphase flow solver using the VOF method within the OpenFOAM (OpenCFD Ltd.) CFD model was used. The governing equations were the Navier-Stokes equation, the continuity equation, and the transport equation of VOF function as shown in the following:

$$\frac{\partial \rho \mathbf{U}}{\partial t} + \nabla \cdot \left(\rho \mathbf{U}\mathbf{U} \right) = -\nabla p + \nabla \cdot \boldsymbol{\tau} + \rho \mathbf{g} + \sigma \kappa \nabla F \tag{2}$$

$$\nabla \cdot \mathbf{U} = 0 \tag{3}$$

$$\frac{\partial F}{\partial t} + \nabla \cdot \left(\mathbf{U}F \right) + \nabla \cdot \left\{ \mathbf{U}_r F \left(1 - F \right) \right\} = 0 \tag{4}$$

where, ρ is the density of the fluid, $\mathbf{U}$ is the velocity vector, p is the pressure, $\boldsymbol{\tau}$ is the viscosity stress tensor, $\mathbf{g}$ is the gravitational acceleration vector, σ is the surface tension coefficient, κ is the curvature of the interface, F is the VOF function, $\mathbf{U}_r$ is the vector in the normal direction of the interface. The left side third term in Eq. (4) was introduced to suppress the numerical diffusion of the VOF function. For the details, see Rusche (2002). The right side fourth term in Eq. (2) represents the surface tension and the model by Brackbill (1992) was used. The density of fluid ρ and the viscosity coefficient of fluid μ were used as the values averaged for each cell as shown below:

$$\rho = F\rho_l + \left(1 - F \right) \rho_g \tag{5}$$

$$\mu = F\mu_l + \left(1 - F \right) \mu_g \tag{6}$$

where, the subscript l and g are the liquid and gas respectively.

The rubble mound was modeled as a porous structure. The hydraulic flow resistance $\mathbf{R}$ in the porous medium was expressed by a Dupuit-Forchheimer relationship as shown below:

$$\mathbf{R} = -\left(\alpha \mathbf{U} + \beta \left| \mathbf{U} \right| \mathbf{U} \right) \tag{7}$$

where, α is the laminar resistance coefficient and β is the turbulent resistance coefficient. These coefficients are expressed using the empirical formulae by Engelund (1953) as follows:

$$\alpha = \alpha_0 \frac{(1-n)^3}{n^2} \frac{\nu}{d^2} \quad , \quad \beta = \beta_0 \frac{1-n}{n^3} \frac{1}{d} \tag{8}$$

where, ν is the kinematic viscosity of water, d is a nominal diameter of the stone, n is the porosity, and α_0 and β_0 are the material constants. Table 2 summarizes the computation method.

Table 2. Numerical analysis method

Software	OpenFOAM CFD model
Basic equations	Navier-Stokes equation of three-dimensional incompressible flow
	Equation of continuity
	Transport equation of VOF function
Solution of free surface	VOF method (two-phase flow model of gas-liquid)
Discretization method	Finite volume method based on unstructured grid
Calculation algorithm	PISO method
Discrete scheme of the transport term	TDV scheme of second-order accuracy
Time integration method	Euler implicit method
Time increment	Automatic control
Maximum Courant number	0.25 or less
Turbulence model	k-ε model
Calculation method of rubble mound	Porous model (the flow resistance is given by a Dupuit-Forchheimer relationship)
Material constants of rubble stone	α_0 = 1500 β_0 = 3.6
Porosity of rubble stone	n = 0.4
Nominal diameter of rubble stone	d = 14.3 mm
Physical property values (index l: liquid, g: gas)	ρ_l = 1000 kg/m^3, ρ_g = 1.0 kg/m^3, μ_l = 1.0×10^{-6} m^2/s, μ_g =1.48×10^{-5} m^2/s, σ = 0.07 N/m

The Finite Volume Method with an unstructured grid was used to reproduce the complicated shape of the armor blocks. Figure 16 shows the bird-eye view of a computational grid. The computation was subdivided into four stages. A two-dimensional calculation was done in Region 1 and Region 2, a three-dimensional calculation was done in the Region 3 and 4 around the blocks. The grid size in the z direction and x direction of Region 1 was set to 1 cm. The grid of the Region 2 was subdivided into one-eighth. This was subdivided in the y direction in Region 3, and further subdivided in the y direction into one-eighth in Region 4.

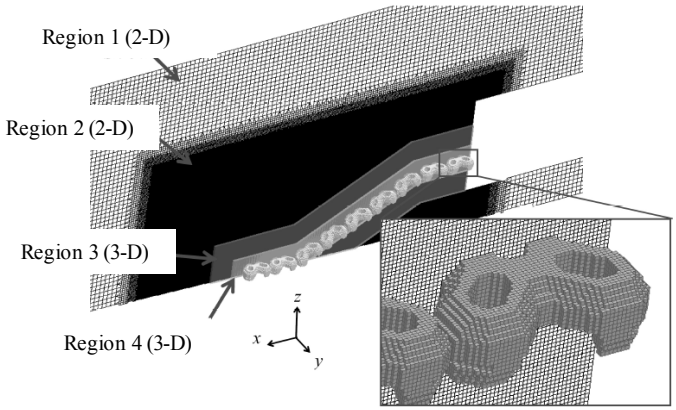

Figure 16. Bird-eye view of computational grid

Tsunami was generated by extruding a wall boundary corresponding to the wave paddle at a prescribed speed as well as the experiments. The computational grid around the wave paddle was moved along with the movement of the wave paddle. This was done by using a moving grid method implemented in the OpenFOAM model.

Firstly, the water jet caused by impinging bore-like tsunami was reproduced. The fluid forces acting on two kinds of blocks, namely, Permex and Permex without holes were then computed to confirm the effect of the well-arranged five holes. Figure 17 shows the shape of each block.

Figure 17. Permex and Permex without holes

Reproduction of experimental water jet caused by impinging bore-like tsunami

Figure 18 shows a comparison of the time-series of water surface elevation at the front face of the caisson. The calculated water surface elevation accurately reproduced the measured one. Figure 19 shows a comparison of the impinging water jet. The water jet impinging onto harbor-side of breakwater was also reproduced accurately.

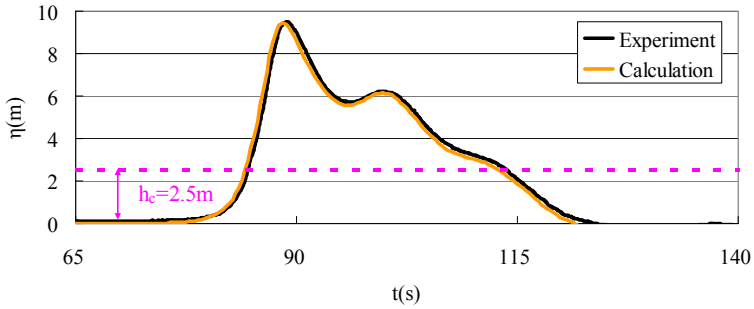

Figure 18. Comparison of the time-series of water surface elevation

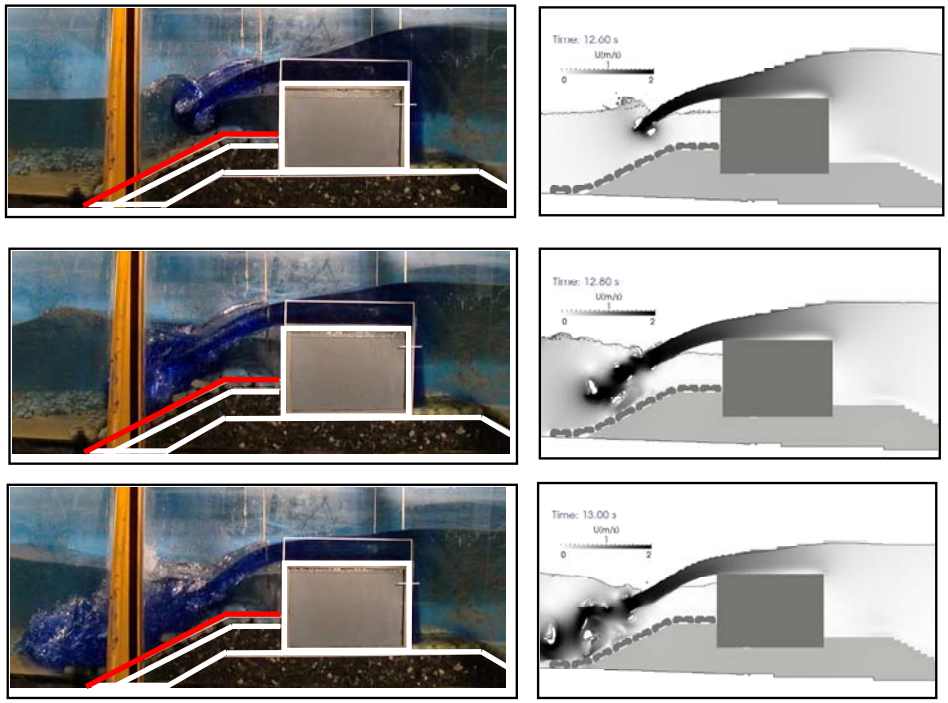

Figure 19. Comparison of the impinging water jet

Fluid forces acting on the blocks

The effect of the holes in the blocks was examined by comparing the fluid force acting on Permex and Permex without holes. Figure 20 shows a hodograph of fluid forces when a counterclockwise vortex was passing through above the block. In Figure 20, the axes refer to the fluid forces acting on the block divided by the underwater weight of the block. It can be seen that the fluid force acting on Permex in the direction away from the slope is smaller than that of Permex without holes. Figure 21 shows iso-pressure line around the blocks when the fluid forces take their maximum value in the direction away from the slope. It can be seen that the pressure difference between the top and bottom surfaces of Permex is small comparing to that of Permex without holes. These results clarify the reason why Permex showed high stability against the water jet in the experiment.

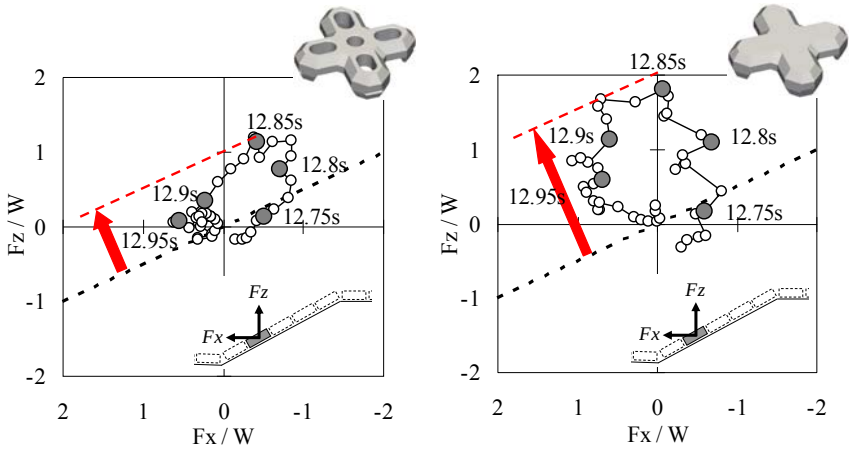

Figure 20. Hodograph of fluid forces acting on the block

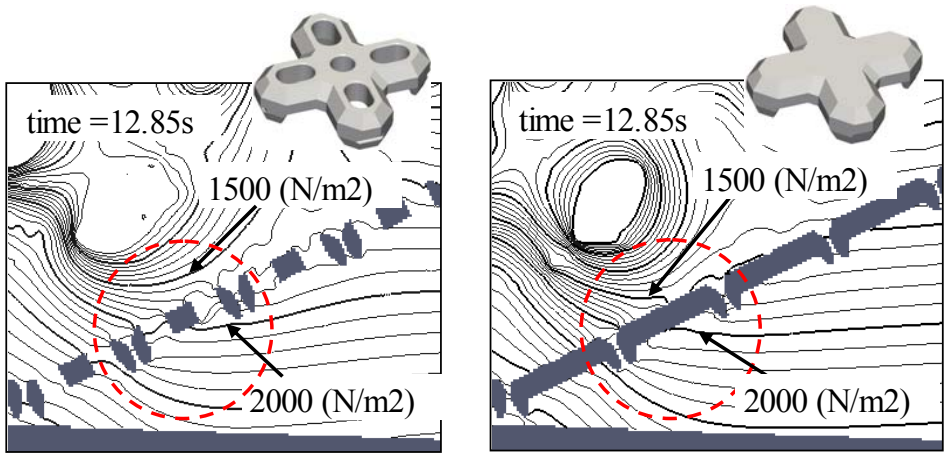

Figure 21. Iso-pressure line around the block

Estimation of lift up of blocks

By using the time series of fluid force acting on the block obtained from the numerical calculation, amount of the lift up of the block was estimated. In this analysis, only the fluid force, buoyant force, and self-weight were considered, but other forces such as the friction force between blocks are disregarded. *Z* and *X* axes are set to normal and tangential direction of the slope. To calculate the displacement of the block, the equation of the motion, which is expressed by the following equation, was solved:

$$m\left(d^2Z/dt^2\right)=F_Z \tag{9}$$

where m is the mass of the block, Z is the displacement of the block in the normal direction, t is the time, F_z is the sum of fluid force, buoyancy and the gravitational force in Z direction. The time series of the block position was obtained by the integration of this equation. Figure 22 shows an example of calculated results. In this case, as for the Permex, no lift up was observed. On the other hand, Permex without holes was lifted in 61mm. By using above method, the analysis of the amount of lift was carried out to compare them with the experimental ones. Figure 23 shows the comparison of experimental and computed damage to the armor blocks. In the Cases1 and 2, X-Block was used, while in the Case3, Permex was used. In the experiment, the damage occurred at the slope in Cases1 and 2. Also in the calculations, lift up above the height of the block was occurred. On the other hand, in Case3, the damage did not occur in the experiment. Similarly, lift up above the height of the block was not observed in the calculations. It can be said that the numerical computation agreed with experimental results qualitatively. However, the position of the damage obtained by the numerical computation was different from the experimental results. Therefore in the future, the applicability of this model has to be improved.

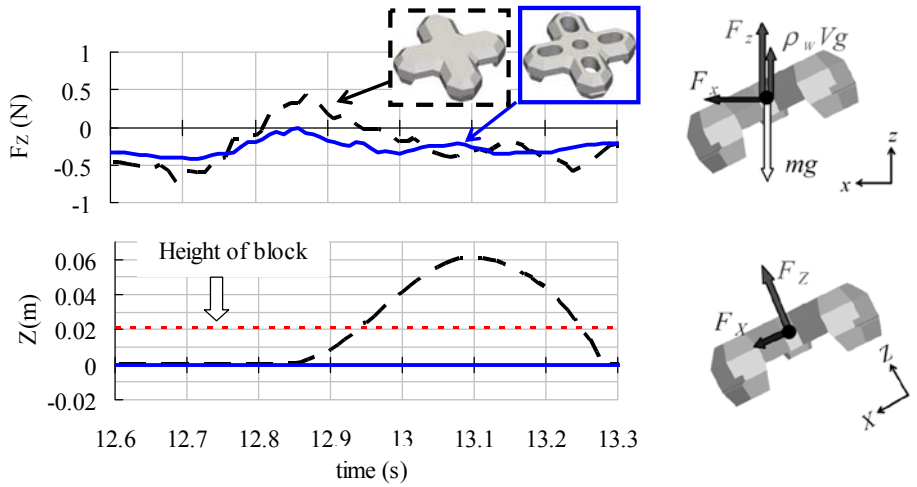

Figure 22. Result of numerical calculation

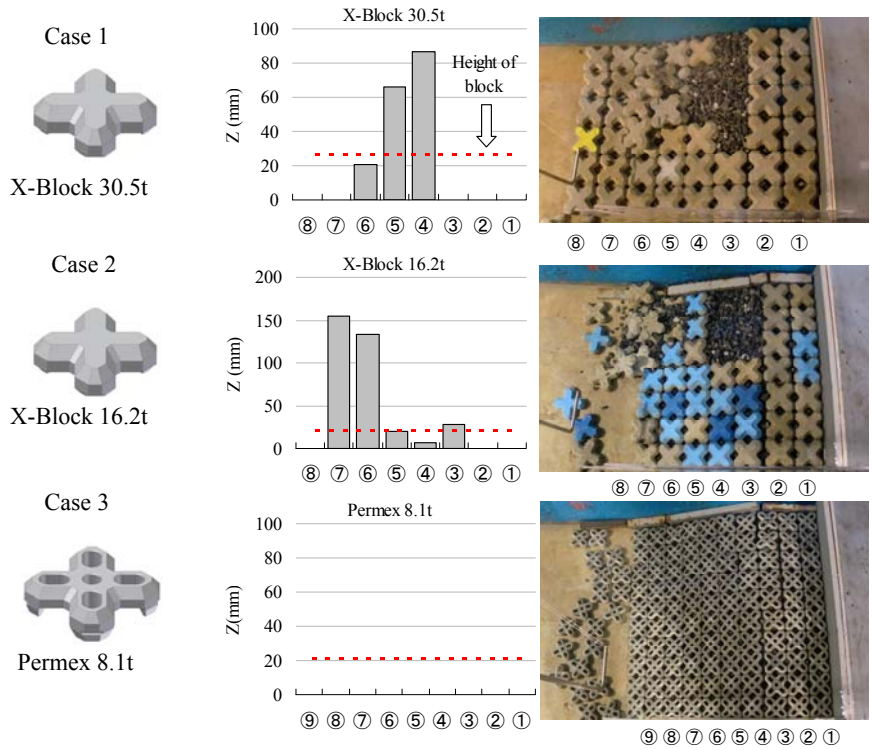

Figure 23. Comparison of experimental and numerical damage to the armor blocks

CONCLUSIONS

A series of hydraulic experiments was carried out to estimate the stability of various types of armor units for a harbor-side rubble mound of composite breakwaters against water jet caused by an impinging bore-like tsunami. The following was found in the experiments:

1. Armor stones of weight 1.0 ton were easily removed by the overflow of the tsunami. They could not secure the stability of the reinforced mound against the water jet.
2. Damage to armor units was strongly dependent on the position of jet impact.
3. The flat type concrete block with well-arranged holes showed high stability against water jet due to the reduction of uplift force.
4. In the case of wave-dissipating blocks, heavier blocks placed along the toe of the slope enhanced the total stability of the armor layer.

Numerical analysis was also conducted to investigate the effect of the shape of the blocks. The following findings were obtained:

5. The wave profile of tsunami and the impinging jet were computed accurately by present method.
6. The effect of well-arranged holes of armor units was verified by computation of fluid forces.
7. Based on the computed fluid force, lift up of blocks was reproduced.

ACKNOWLEDGMENTS

The authors would like to express their sincere gratitude to Prof. Nobuhisa Kobayashi, University of Delaware, for his helpful advice on this study.

REFERENCES

Arikawa, T., M. Sato, K. Shimosako, T. Tomita, G. Yeom, and T. Niwa. 2013. Failure mechanism and resiliency of breakwaters under tsunami, *Technical Note of the Port and Airport Research Institute*, No. 1269 (in Japanese).

Brackbill, J.U., D.B. Kothe, and C. Zemach. 1992. A continuum method for modeling surface tension, *J. Comp. Phys.*, Vol. 100, 335-354.

Engelund, F. 1953. On the laminar and turbulent flows of ground water through homogeneous sand, *Transactions of the Danish Academy of Technical Sciences*, Vol. 3, No. 4.

Hamaguchi, M., S. Kubota, A. Matsumoto, M. Hanzawa, M. Yamamoto, H. Moritaka, and K. Shimosako. 2007. Hydraulic stability of new flat type armor block with very large openings for use in composite breakwater rubble mound protection, *Proceedings of Coastal Structures 2007*, ASCE, 116-127.

Kubota, S., M. Hamaguchi, A. Matsumoto, M. Hanzawa, and M. Yamamoto. 2008. Wave force and stability of new flat type concrete block with large openings for submerged breakwaters, *Proceedings of 31st International Conference on Coastal Engineering*, ASCE, 3423-3435.

Ministry of Land, Infrastructure, Transport and Tourism, Port and Harbor Bureau. 2013. Design guideline of breakwaters against tsunami (in Japanese).

OpenCFD Ltd. OpenFOAM User Guide version 2.0.1, http://www.openfoam.com.

Rusche, H. 2002. Computational fluid dynamics of dispersed two-phase flows at high phase fractions, *Ph.D. thesis*, Imperial College, University of London.